

Identifying Triplicated P-phase Arrivals in Amphibious Seismic Data to Explore the Mantle Transition
Zone

By Auden Reid-McLaughlin
Advisor: Geoffrey Abers, Earth and Atmospheric Sciences
Funding: James Moore '62 EE
August 18, 2021

Abstract:

The Mantle Transition Zone (MTZ) is the physical and chemical transitional layer that separates the Lower and Upper Mantle between depths of 410 and 660 kilometers. Seismograms recorded between 10 and 30 degrees epicentral from seismic events show clear evidence of rays traveling through these upper mantle discontinuities, known as triplication. Identifying triplicated P-phases in seismic arrival data allows seismologists to constrain features of the MTZ through waveform modeling, as differences in expected and observed travel times yield information about the exact ray paths taken such as depth of discontinuity and vertical heterogeneity. The Alaska Peninsula is an optimal region of study, due to the subduction of the Pacific Plate under the North American Plate, giving rise to significant seismic activity. The deployment of both onshore and ocean bottom seismometers during the Alaska Amphibious Community Seismic Experiment (AACSE) has gathered fifteen months of seismic data from which this project draws. After identifying suitable events for the study, the project discerns and enhances these triplication patterns from the amphibious data using array processing techniques such as filtering, stacking, beamforming, frequency wavenumber analysis, and cross correlation. The paper goes on to discuss the specific challenges with ocean bottom seismometer data, as well as effects from volcanic structures on arrival data while using the listed techniques to rectify these obstacles. This identification would be important to the field of earth science, as it would advance the understanding of Earth's internal processes by better understanding key features of its structure. Currently, there is much speculation as to the origin of volcanic activity and magmas which seem unrelated to known processes of volcanism. Many theories involve the MTZ, characterizing a new class of volcanism that originates in this zone which would be greatly aided by an accurate model of the region.

Introduction:

As shown in the figure below (1a), the distance range from 10 to 30 degrees encompasses two branches of triplication, the first from the 410 discontinuity and the second from the 660. The figure describes the travel time, or time it takes for the wave to reach a certain distance, as a function of distance from the source. As is shown, at a given distance there can be as few as one P-wave arrival, or as many as 5, where the two triplicated branches overlap (around 20 degrees epicentral distance).

The reason for this triplication is shown in figure 1b, which plots the ray paths of the three separate waves from one source (a single event) that generate the pattern seen in 1a according to the IASP91 model of the subsurface. First, the direct ray, which does not pass through the 410 discontinuity, and goes directly to the seismic station that receives the signal. Second, the reflected ray, which reaches the 410 discontinuity and bounces off, and then continues its path to the receiver. Third, the refracted ray, which reaches the 410 and is subsequently refracted through, curving back up underneath the discontinuity and refracted once again on its upgoing path through the discontinuity, then continuing through the upper mantle to the receiver. The same is for the 660 discontinuity. Clearly, each ray will eventually make it to the receiver at different times, as they take different paths. Figure 1b shows that a receiver at an epicentral distance of 20 degrees from an event should theoretically record 5 p-wave arrivals, which is again shown in 1a. Both figures were generated using the IASP91 model for an event with a depth of 50 kilometers.

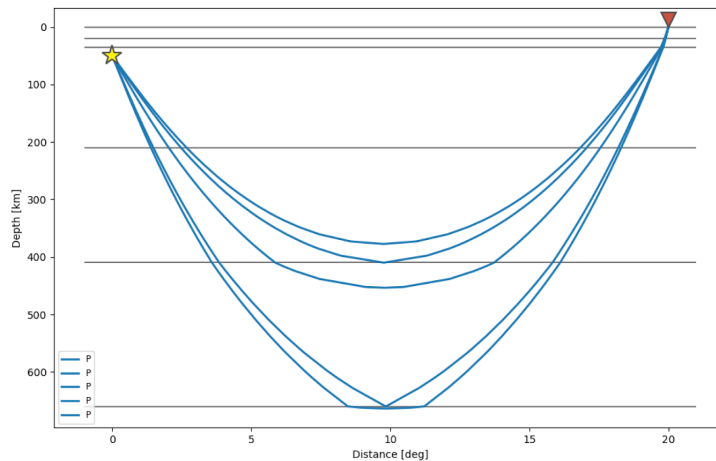
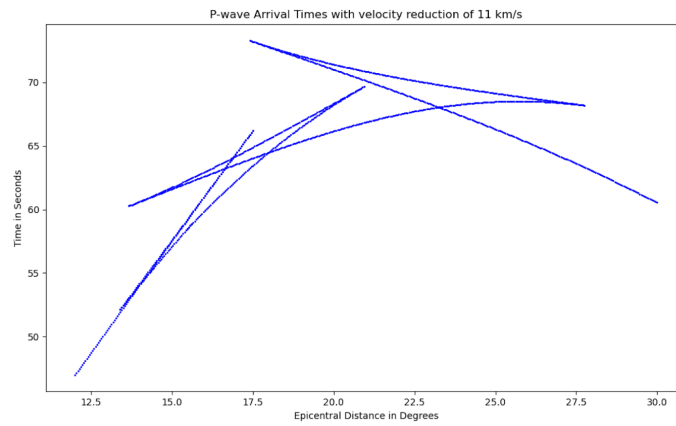


Figure 1: a) P-phase travel times with velocity reduction of 11 km/s for a source with depth of 50 km, b) Ray paths of P wave from source with depth of 50 km according to IASP91 Earth Model

The AACSE array, shown in Figure 2, is an amphibious array that has gathered seismic data over 15 months on and off the coast of Alaska. This region has been an area of extreme interest to the seismology community for decades do both subduction and volcanism that causes significant seismic activity that has been historically used to help image the subsurface. The orange hyphenated regions represent some of these historic earthquakes and aftershock sequences. Recently, there have been several notable earthquakes in the region, including a Magnitude 7.8 and 7.6 in 2020, as well as an 8.2 earlier this summer. Unfortunately, the AACSE array is not currently deployed and did not record these events, but the permanent stations in the region collected seismic data. Regardless, these events illustrate exactly the reason for research into the internal structure of the Earth in this zone. A dense array such as AACSE is deployed with the purpose of constraining features of the subsurface by minimizing undersampling of the region. Specifically, in the case of AACSE, ocean bottom seismometers are used to collect data on historically undersampled regions, as well as, in the case of triplication, avoid shallow subsurface heterogeneities that attenuate seismic signal.

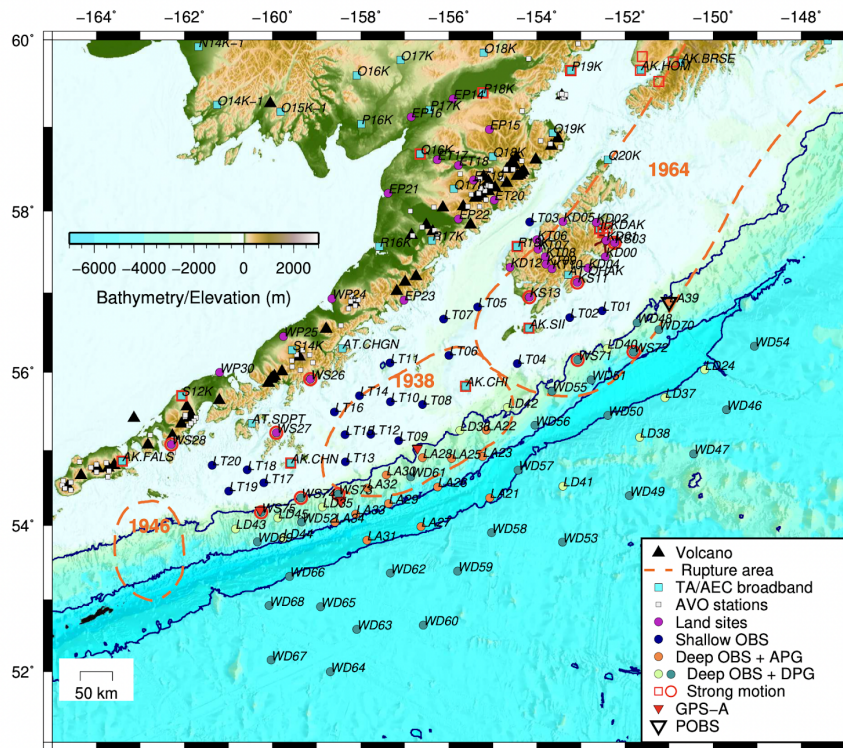


Figure 2: The AACSE Array in Alaska

The purpose of this project is to use both the onshore and offshore seismic data to discern triplication patterns as described above. This paper will go on to show why the ocean bottom seismometers require a different approach than those on land, and how it is possible to identify the triplicated phases in the on land data using well known array processing techniques.

Materials and Methods:

The majority of the project was able to be completed on a laptop computer, while some programs which require more computing power were run on a desktop computer.

The first step in the project was to survey all the seismic events, henceforth referred to as events, during the given time period that the AACSE array was deployed to identify events that are suitable for the analysis. The time frame which was searched spans from May 10th 2018 to September 10th 2019.

The first round of searching involved surveying all events from 8 to 18 degrees away from the center of the seismic array and was later expanded to 25 degrees. This distance range is due to the ray path of the seismic waves. Referring to Figure 1 above, these distance ranges include both the 410 and 660 triplication branches.

There are several other factors that influence the appearance of these triplicated P-wave arrivals on a seismogram. As the wave propagates outward from the source, due to attenuation from the mantle material, it loses energy (and therefore amplitude) the longer it stays in the mantle, meaning that for small

events (magnitude 5 and below), it is unlikely that the later arrivals will show as clearly, if at all, on the seismogram. Thus, only events in the given time and distance range that were above a magnitude 5 were analyzed. This is not to say that all magnitude 5 and above events will show triplication in the arrival data, as other factors such as differences in depth and location can cause rays to move through heterogeneities in the mantle which attenuate the signal. Using IRIS catalog search, these events were downloaded into a QuakeML format that can be read using built-in ObsPy functions. Obspy is a python based open source project that seismologists can use as a tool to process certain seismological data, and it was used for many of the basic filtering and processing tasks over the course of this project.

Once the event catalog was downloaded, individual seismograms from the stations in the AACSE array were downloaded as well to construct record sections of the event in our given area of interest. These seismograms were filtered using a bandpass filter, meaning that a minimum and maximum frequency were set, and only the frequencies between these values were shown in the waveform. This is done so as to maximize the signal to background noise and more clearly show the given arrivals of interest. The seismometers deployed are known as broadband seismometers which gather signals on a broad range of frequencies, meaning this filtering step is incredibly important to isolate the specific wave arrivals. Furthermore, different waves have different frequency bands at which they are most prominent, and this physical attribute can be used to guide the filtering process.

To help guide this process and help identify triplicated arrivals in the seismograms, synthetic seismograms were downloaded to underlay the observed waveforms. These synthetics were generated from the Global Centroid Moment Tensor project through IRIS, and are only available for certain seismic events, which happen to be large earthquakes. These synthetics are generated at a period of 2-100 s, i.e. very low frequencies, meaning that P-wave triplications are very clear on their waveforms. These synthetics also help to highlight the differences in arrival times, making them very useful for later analysis. Shown in Figure 3 below is the record section for an event filtered between 0.01 and 0.4 Hz with the observed waveforms in red, the synthetic waveforms in grey, and the predicted P-wave arrivals overlaid on the section in blue.

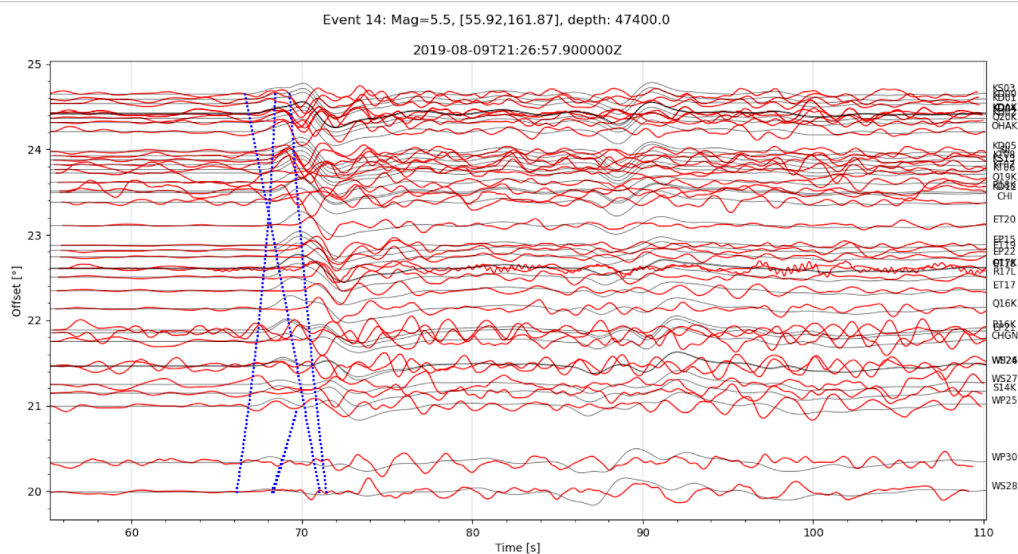


Figure 3: Record section for Event 14 with velocity reduction of 11 km/s. The observed seismograms are shown in red, the synthetics in grey, and the predicted p wave arrivals in blue. At this distance, the 660 branch of triplication is shown.

Analysis Methods:

Once suitable events were identified and filtered, analysis of these events and waveforms ensued. Array analysis techniques were applied to these waveforms to further enhance the signal so as to 1) identify the P arrivals and 2) gather seismological information on the region of the array.

This can be done in a physical sense, by first assuming that the wave arriving at the array is an elastic plane wave. The wave recorded at the center of the seismic array from the plane wave can be modeled by the following equation:

$$x_{center} = f(t) + n_i(t)$$

where $f(t)$ describes the signal and $n(t)$ describes the noise. Due to the difference in location of each station, individual seismometers record the waveform according to the following:

$$x_i = f(t - \overline{r}_i \cdot \overline{u}_{hor}) + n_i(t)$$

where \overline{r}_i represents the location vector of the seismometer relative to the center of the array, and \overline{u}_{hor} represents the horizontal slowness vector, which is a physical attribute of the subsurface and represents the reciprocal of velocity in the horizontal direction. The dot product of these vectors works out to be the time shift of wave arrivals at each seismic station.

The first technique applied is known as waveform stacking. Simply put, the two waveforms which are nearest to each other in distance are added together to get one signal. This is then done with all the waveforms in the array with their nearest neighbors. The idea is that by doing this, any waveform coherence will be amplified, while incoherence will be relatively quiet. This technique is the most basic form of array analysis, but it gives a good indication as to whether or not coherence between waveforms exists.

The process known as beamforming is the same process as wave stacking, only the time shift between the nearest neighbors due to both the slowness and location as described above, is removed according to the following:

$$\overline{x}_i = x_i(t + \overline{r}_i \cdot \overline{u}_{hor}) = f(t) + n_i(t + \overline{r}_i \cdot \overline{u}_{hor})$$

Using known velocity models, i.e. IASP91 as used in this project, the horizontal slowness of the subsurface can be approximated and used to apply this time shift to the seismograms, ideally aligning the wave arrivals for summation, amplifying the signal even further. The difference in simple wave stacking and beamforming is illustrated in the figure below.

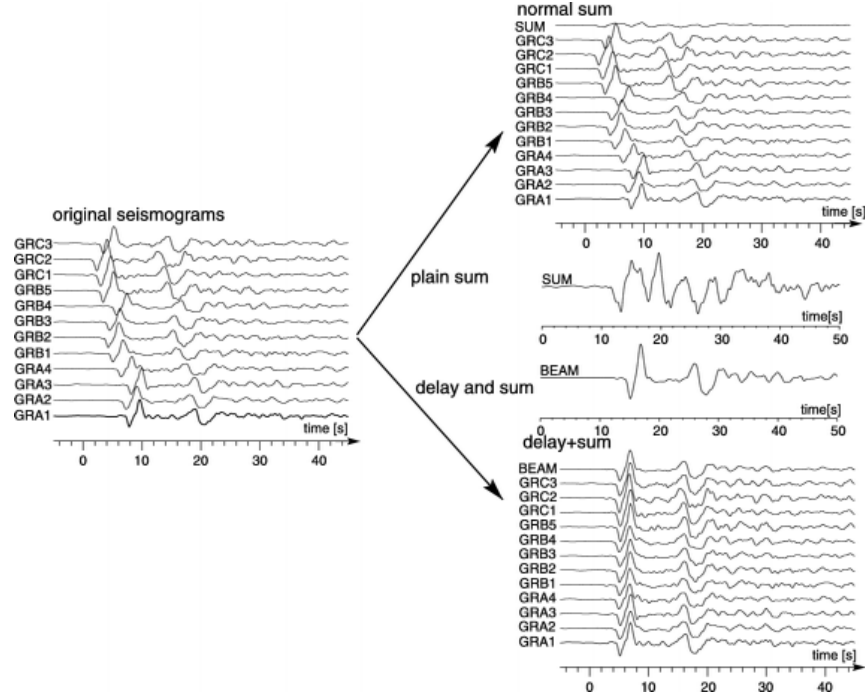


Figure 4: Summing methods for waveform stacking, from Array Seismology: Methods and Applications (2002)

Beamforming, also known as the delay and sum method, results in a sharper signal in which individual wave arrivals can be more clearly observed, allowing triplicated patterns to become more apparent. The improvement in signal to noise ratio is a factor of the square root of the number of stations in the array. The next method used is called frequency wavenumber analysis, or more specifically in this project sliding window fk analysis which operates over longer time scales, i.e. the entire waveform as opposed to a single arrival. This analysis works by essentially performing a beamforming analysis over a range of slownesses, rather than assuming a given slowness according to an Earth model. It does this by using the total energy recorded from an array, given by the following:

$$y(t) = \frac{1}{N} \sum_{n=1}^N x_n(t + \overline{r}_n \cdot \overline{u}_{hor})$$

$$E(u) = \int_{-\infty}^{\infty} y^2(t) dt$$

where y describes the summed signals from beamforming at a given slowness.

The analysis takes place in the fourier, or frequency domain, and can be described as follows:

$$E(k) = \frac{1}{2\pi} \int_{-\infty}^{\infty} S(w)^2 A(\overline{k})^2 dw$$

$$\overline{k} = w * \overline{u} = \frac{w}{v_0} (\cos\theta, \sin\theta)$$

where S(w) is the fourier transform of the signal to the frequency domain, A(k) is the array response function, which is proportional to the amplitude of the signal, and k is the wavenumber, which is related to the slowness of the subsurface, u, and back azimuth of the source, θ (i.e. the angle from North of the seismic station relative to the source location).

Therefore, both the slowness and back azimuth can be calculated from the wavenumber. The energy calculation is carried out over a range of wavenumbers and displayed as an energy or power over space for fk analysis. For the sliding window, as said before, the analysis involves a time series, and is therefore displayed as power versus time, and can therefore be shown as back azimuth and/or slowness versus time, as shown in the figure below.

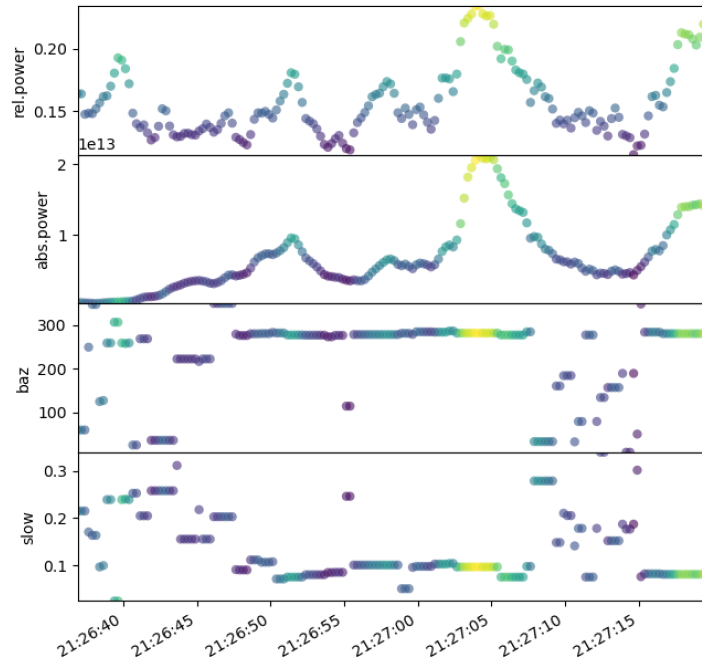


Figure 5: Output of sliding window FK Analysis on waveforms

Since the energy (and power) are proportional to the squared amplitude of the beamformed arrays, the power peak gives a good indication of not only where in time the arrivals occur, but at which slowness and back azimuth these power peaks are found. This yields information about both the individual wave arrivals as well as the subsurface and source of the waves themselves. The calculated values can help relocate seismic events, as well as act as a sanity check when the back azimuth and slowness are already known or well constrained.

The third analysis technique builds off of fk analysis and is known as slant stacking, or vespagrams. This technique follows the same exact process as sliding window fk analysis, but where fk analysis only takes the maximum power found at a given time, vespagrams display the power density as a function of both time and slowness or back azimuth. If the vespagram displays a function of slowness, the back azimuth is set, and vice versa. Using the back azimuths at which the power peaks in the fk diagrams, the slant stack is carried out for a range of slownesses at the given back azimuthal angle, and displayed as shown below.

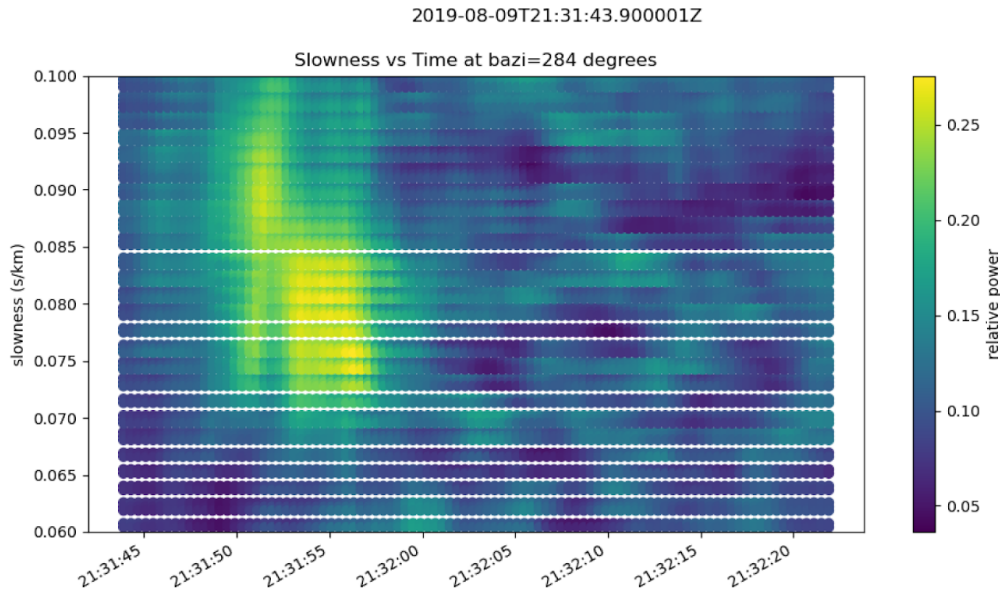


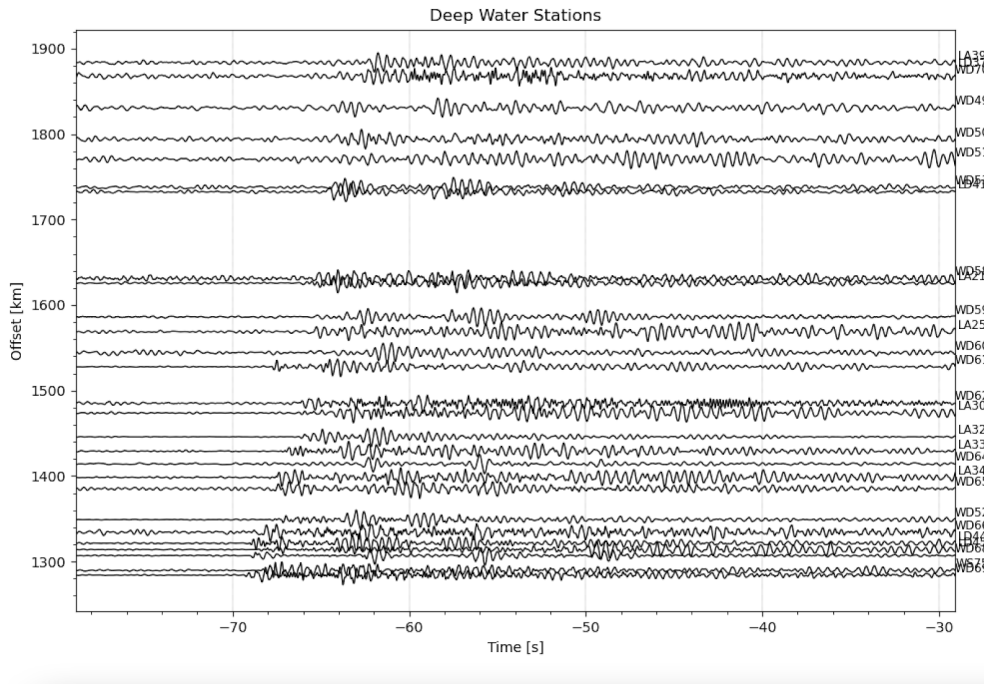
Figure 6: Example Vesogram from Event 14 with back azimuth=284 degrees

The benefit of the vesogram calculation is that it much more clearly illustrates multiple phase arrivals that occur closely together, where the fk diagram does not differentiate between them as clearly. With power peaks at several different slowness values, phases can be differentiated due to the path they take through the mantle. Referring back to Figure 1a, as slowness is the reciprocal of velocity, the slope of the triplication branches reveals the slownesses at which each triplicated phase should arrive according to a given earth model, or at least relative to the other p-arrivals. For the 410 branch, the first p arrival should have a higher slowness than the second and third as its slope is steeper before the triplicated point. The calculation of slowness for a given phase arrival is vital for generating and developing earth models as well.

The final analysis technique is called cross correlation. Cross correlation is the measure of similarity between two signals as a function of displacement of one relative to another. In terms of seismology, a window around a phase arrival can be drawn on a seismogram, and this window can be moved along another seismogram from the same source. Ideally, if they've taken the same or similar paths, similarity between the signals will be found at an offset in time with a calculated coefficient of correlation that describes the degree of similarity, with -1 being complete incoherence and 1 being complete coherence. For this project, the seismograms for the chosen events were cross correlated with their synthetics, a technique introduced in Chu et. al 2012, where the cross correlation was used to illustrate the regional attenuation of signals at some seismic stations to others, and apply the time shifts calculated as corrections to rid these regional effects so as to reveal the deep branches traveled by the ray paths. Not only can this technique improve wave coherence across an array, but it also reveals information about the regional structure of the subsurface around given stations.

Results:

Through the initial process of filtering, the seismic stations were split into four different record sections based on elevation in order to identify patterns in the arrival behavior of the waves that may be dependent on this location, as well as see their response to different filter bands. Immediately, a pattern in the ocean bottom seismometers appeared. Two of these record sections are displayed below for a single event, to illustrate a pattern discovered in the deep water stations i.e. deeper than 100 meters(OBS stations in Figure 2). These sections are filtered with a bandpass filter between 2 and 3 Hz, and a velocity reduction of 10 km/second has been applied. As is clear in several of the seismogram traces, there appears to be a periodicity in signal for many of the stations, particularly the WDs. Looking at the trace for WD68, the signal similar in amplitude and length to the initial P-wave arrival seems to repeat every 6 or 7 seconds. Comparing this to the land stations, i.e. elevation above 0 meters, this periodicity is non apparent, or rather non existent. This periodicity is consistent with that of the period of the water column, propagating the wave up and back down again and causing this repeat signal. This makes using the OBS' for analysis a more difficult task without further filtering and response removal. Due to this, during later analyses of the phase arrivals, the project focused more on the shallow water and land stations.



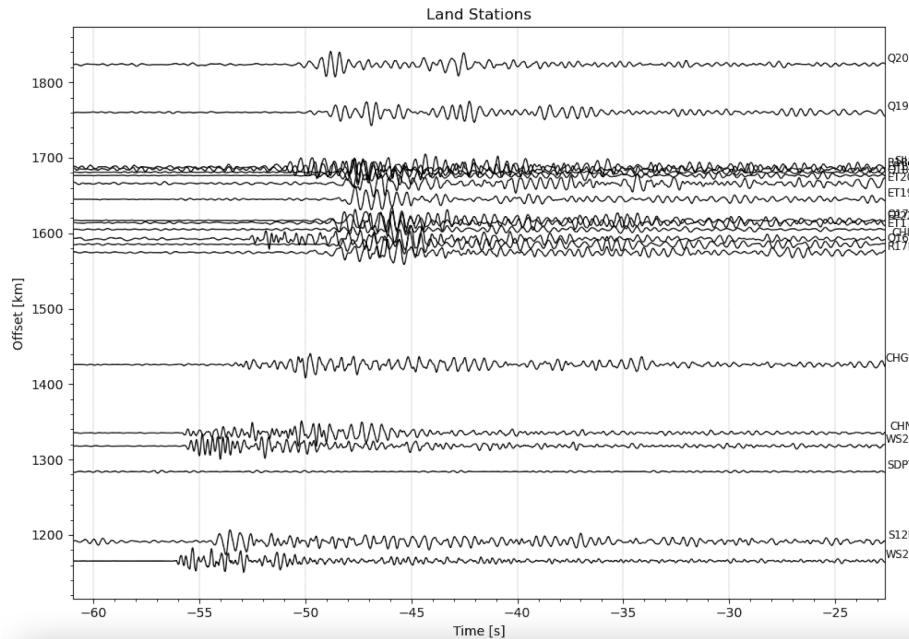
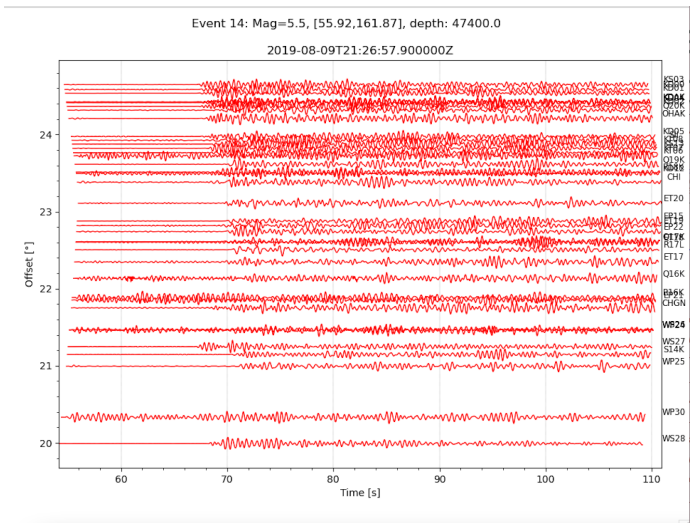
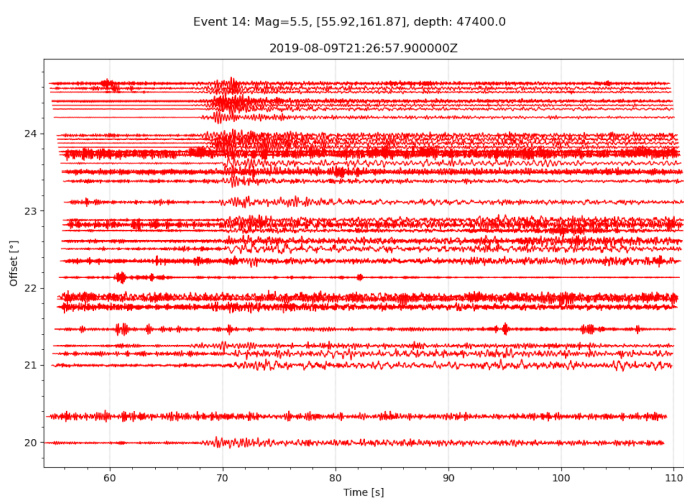


Figure 7: a) record section of Deep Water Stations (OBS) where arrival periodicity from water column is clear, b) record section of land stations for comparison

After extensive filtering, a frequency band of 0.01 to 0.5 Hz appeared to show the most clear signal for the arrivals. This was determined by apparent coherence in the waveforms, and consistent with the seismological literature, which details that P-waves have a dominant signal at very low frequencies. Shown in figure 2 below are three record sections for three different frequency bands for some of the AACSE stations. Figure 8c shows a band of 0.01 to 0.4 Hz, the band that was used for the rest of the project. As is shown in Figure 8c, coherence in the first P arrival is significantly clearer than the other two bandpass filters, where the troughs align very closely to form a near continuous arrival line.



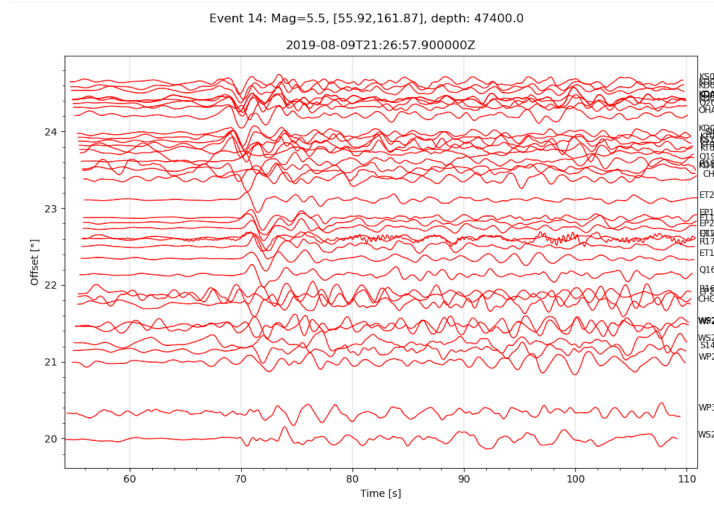


Figure 8: Record sections for three different frequency bands a) 5-8 Hz, b) 2-3 Hz, c) 0.01-0.4 Hz

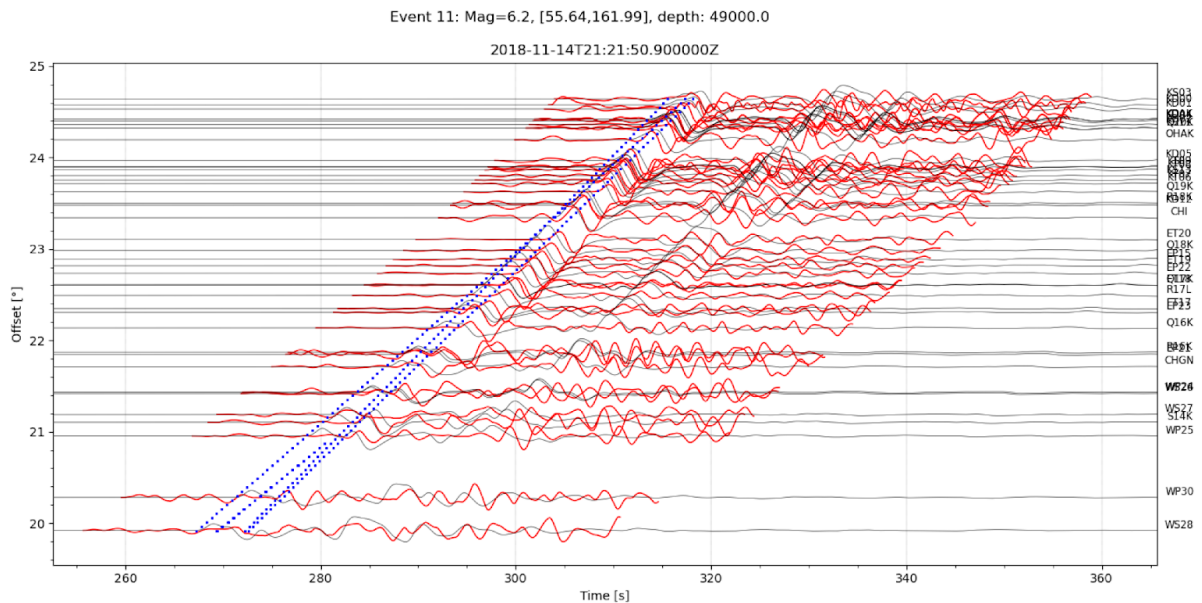
Through this processing and filtering, two events were identified as containing enough signal to analyze. These events will be referred to as Event 11 and Event 14, whose stats are displayed in the table below. Both events took place on the eastern coast of the Kamchatka Peninsula, between 20 and 25 degrees from the center of the AACSE array, as illustrated in the map, where the contours refer to 10, 15, 20, and 25 degrees from the center respectively.

Event	Time (Y-M-D: T)	Longitude	Latitude	Depth (km)	Magnitude (Mw)
11	2018-11-14: 21:21:50.900	161.99	55.64	49.0	6.2
14	2019-08-09: 21:26:57.900	161.87	55.92	47.4	5.5



Figure 9: a) table with earthquake data from events 11 and 14, b) location of events 11 and 14 relative to the center of the AACSE array, where contour lines represent 10, 15, 20 and 25 degrees epicentrally

The record sections for the two events along with their synthetics and triplication layovers are displayed below, filtered between 0.04 and 0.4 Hz. Due to their distance from the array (around 23 degrees), the triplication branch for the 660 km discontinuity will have arrivals on this particular record section, as well as the tail end of the 410 branch. This is shown in the triplication layover in blue.



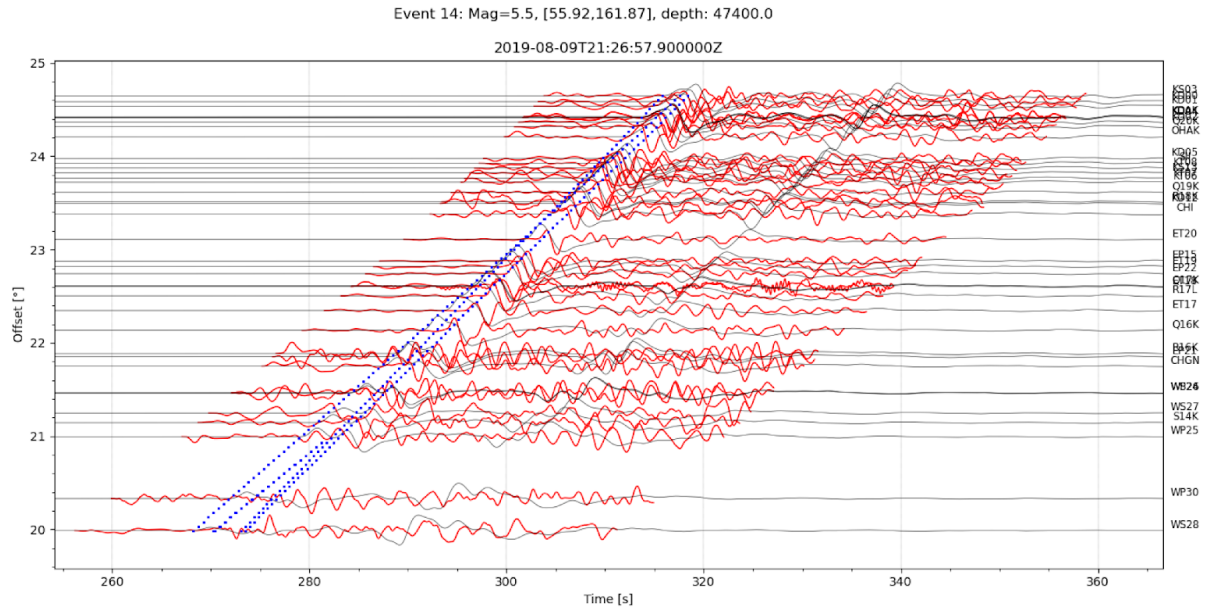


Figure 10: Record sections for event 11 and event 14, with observed waveforms shown in red, synthetics shown in grey, and expected P arrivals from IASP91 shown in blue (660 triplication branch)

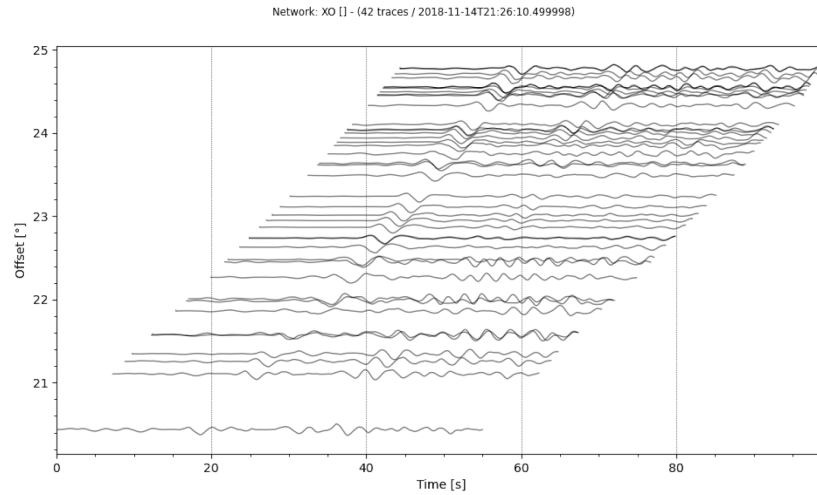
There are several things to note. First, due to the size of Event 11, the signal to noise ratio is much higher, yielding a smoother trace before the first P-arrival. The trace is quicker to quiet down as well for this event. Comparatively, Event 14 shows significant noise for several of the stations before the P-wave arrival, specifically for the EP and R stations.

Secondly, though the triplicated layover and synthetics act as a helpful guide, it is difficult to discern between triplicated P-wave arrivals in the recorded traces, if they exist at all.

Thirdly, there seems to be a clear and consistent pattern in the first p-wave arrival across both events, where the stations between 22 and 23 degrees have a significantly delayed arrival time compared to the rest of the first arrivals. This is clear when laid over the synthetic. Looking at ET20 for both events, the synthetic crest appears nearly a second before the observed crest, and this is consistent for the following traces until 22 degrees, which all correspond to land stations (not including Kodiak Island stations). Due to the first two observations, it is necessary to perform further analysis to amplify the signal of the arrivals.

The results of the nearest neighbor waveform stacking are shown below in Figure 11. For both events, the stacking succeeded in smoothing the traces and therefore reducing noise. Further, not only was the initial P arrival amplified, but later arrivals which were originally lost in the noise now appear to have coherence, showing two, possibly three clear peaks in addition to the first, larger arrival in Event 11. Event 14 shows these later phases less consistently. However, as discussed in the methods section, the limitations of the simple stacking technique can diminish the sharpness of the signals, so while coherence has become enhanced, three separate P arrivals from triplication are unable to be discerned.

Event 11:



Event 14:

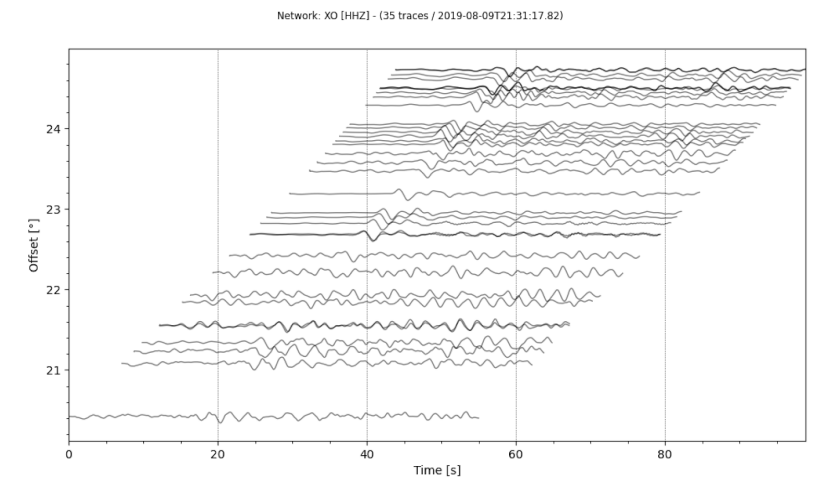
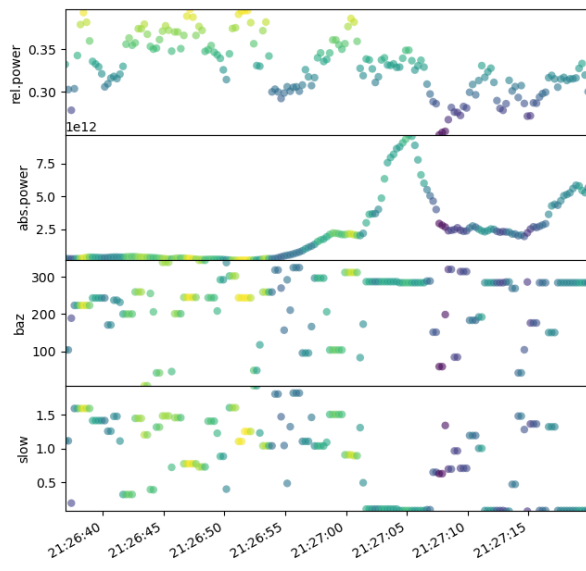
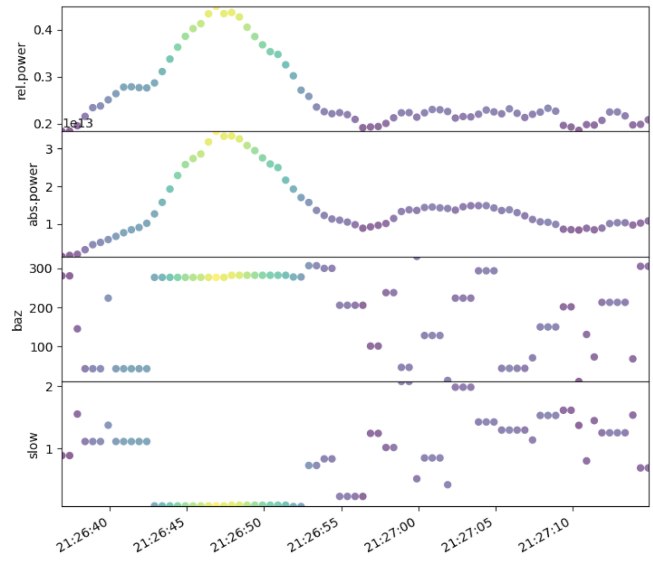


Figure 11: Results from nearest neighbor waveform stacking. Smoothing is clear, as well as secondary phase arrivals later on in the signal

FK analysis was applied next. Due to the consistent pattern of delay in arrival times for the land stations, the stations were filtered into two categories before applying the analysis: Land Stations (EP, ET, and Q stations), and Island Stations (KD, KT, and KS stations). The results of the analysis on Event 11 are displayed in Figure 12.



Island Stations



Land Stations

Figure 12: Results of FK analysis for event 11 shown for island and land stations

The analyses show a peak in absolute power at different times for each set of stations. The Island stations see a peak nearly 30 seconds after the event, whereas the land stations see their peak around 10 seconds after the event, and this is consistent in their distance from the source. Looking at the original record sections for the event, there should be around a 20-30 second difference between the first P-wave arrival at the closest land station and the first P-wave arrival at the furthest island station. Recall that fk analysis completes beamforming over a range of slownesses, and therefore the presence of one central peak implies that the beamforming at the slowness that corresponds implies coherence in the signal. Zooming in on the slowness and back azimuth plots around the time of the central power peak, it becomes clear that there are actually multiple power peaks, as shown in Figure 13, which show the slowness and back azimuth of the land stations for Event 14. These power peaks are at a slowness of 0.092 s/km and 0.083 s/km, and back azimuths of 283 and 284 degrees respectively. For reference, the back azimuthal angle from the event to the center of the array is around 284 degrees. In these figures, there seem to be two peaks with high relative power, and a possible third with slightly diminished power. This prompted a vesogram analysis to view the full spectrum of power density around these peaks.

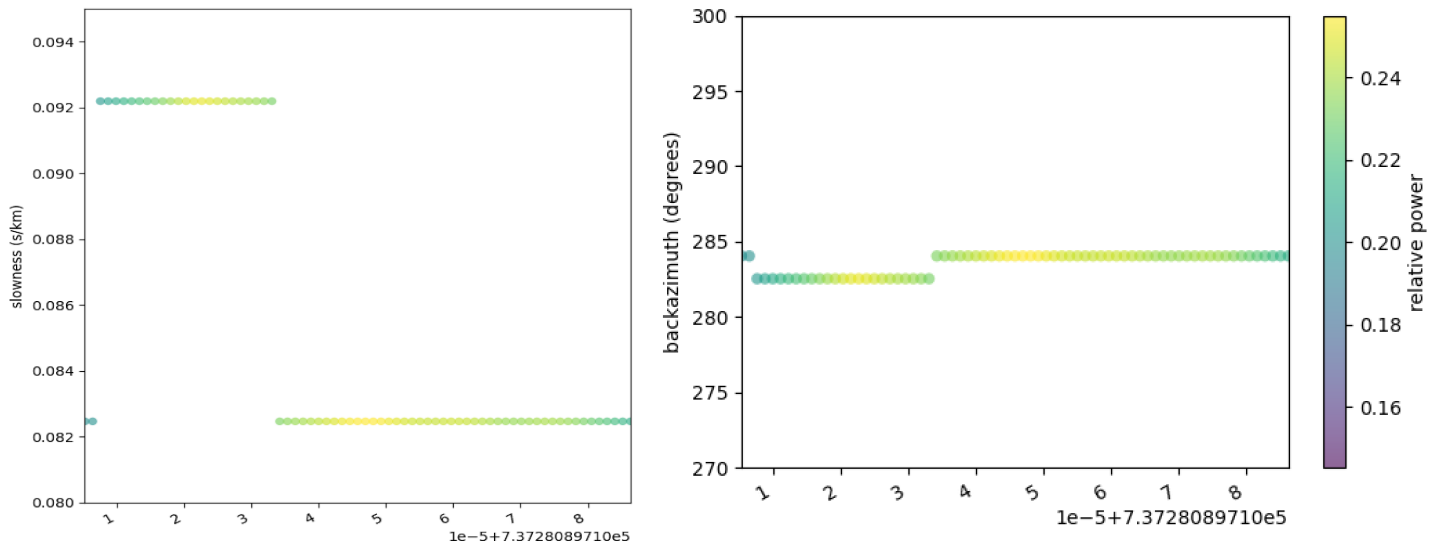


Figure 13: Back azimuth and slowness fk analysis results zoomed in around the power peaks

The vespagram analysis yielded the plot shown in Figure 14. Since the vespagram analysis is most accurate when done over a very small range of back azimuths, a range from 283-285 degrees was used in the analysis. This is because, as seen in Figure 13, there are two azimuthal angles with power peaks. The plot shows the vespagram for Event 14 at a back azimuth of 283 to 285 degrees. There are clearly several power peaks, one around slowness 0.092, and two others at a less well constrained range of around 0.08 s/km. These peaks occur within 5 seconds of each other, with the first arrival around 293 seconds after the event. The two secondary peaks are slightly more difficult to discern in the vespagram, but the first is much more well defined over a small range of slownesses.

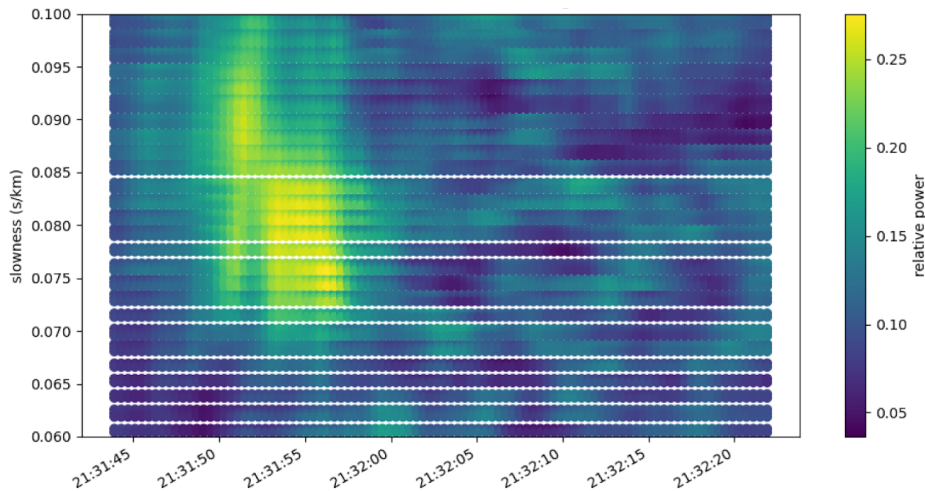
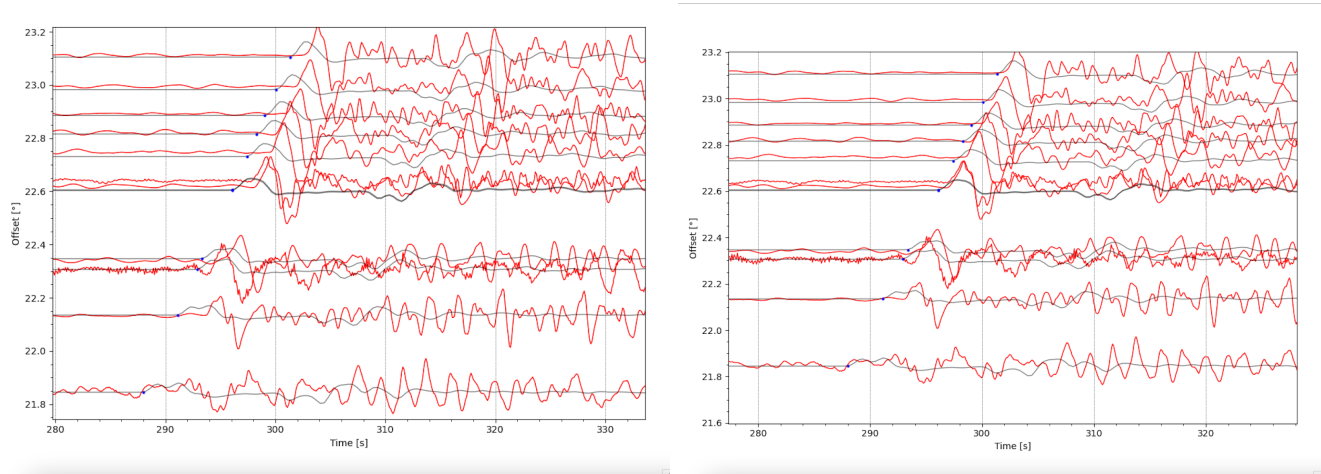


Figure 14: Vespagram result for the land stations on event 14

To address the other main observation of the record sections, the delay times of the land stations, the cross correlation with synthetics as described in the methods section was carried out on the waveforms. The record sections for the land stations with the synthetic underlay before and after the cross

correlation time shift has been applied are displayed in Figure 15. The cross correlation is applied to all stations used in the analysis, but only the land stations are shown here as they are the waveforms with the notable delay. The time shifts and correlation coefficients are shown in the matrix for the respective traces. Clearly, there are significant time shifts calculated by the cross correlation. Once these time shifts are applied, the first observed P-wave arrival appears much closer to the predicted arrival time according to IASP91, shown as a blue dot.

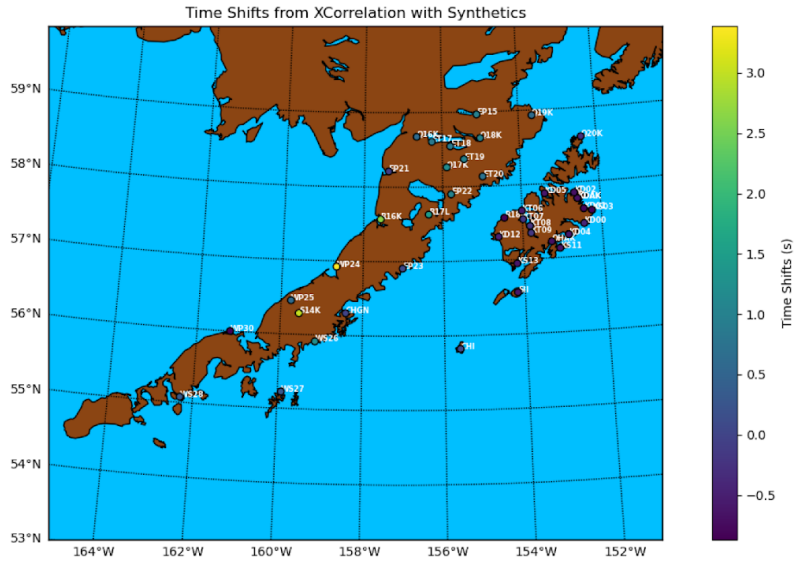


```
[ (0.96465686016170549, 0.76517733191183523),
  (-0.070910428387052762, 0.23530016664818415),
  (1.0454987856010778, 0.68314244877847019),
  (0.065861748048375329, 0.82545727772292143),
  (0.84736891736744124, 0.60269661528583907),
  (0.87597542688195174, 0.72369090166705485),
  (0.99407897249322352, 0.74968525200233227),
  (0.73328427295380894, 0.88772595217772166),
  (0.6104361347172671, 0.3943657500733917),
  (1.1728210983838205, 0.5843011900052657),
  (1.0396784601236126, 0.79607956951397796),
  (0.62532072786049608, 0.88170707849673924),
  (-0.33313953077145858, 0.92954867842353261) ]
```

Figure 15: a) record section of land stations for event 14 before cross correlations time shift applied, b) same record section with time shift applied, c) matrix showing time shifts (column 1), and correlation coefficients (column 2)

This cross correlation was run for both events on all land and island stations, and the time shifts were plotted on maps in an attempt to better recognize a pattern in the regional structure. These results are twofold: 1) the land stations do in fact have a recognizable delay pattern with respect to the other stations, particularly the island stations, with as much as a 3 second time shift subtracted to the original waveform, and 2) the island stations, according to the cross correlation, require a time shift in the positive direction for Event 14, meaning that they experienced arrivals earlier than expected from the synthetics. This negative delay for the island stations is not as severe as the positive delay for the land stations in Event 11, but it is still noticeable.

Event 11: 2018-11-14T21:21:50.900000Z



Event 14: 2019-08-09T21:26:57.900000Z

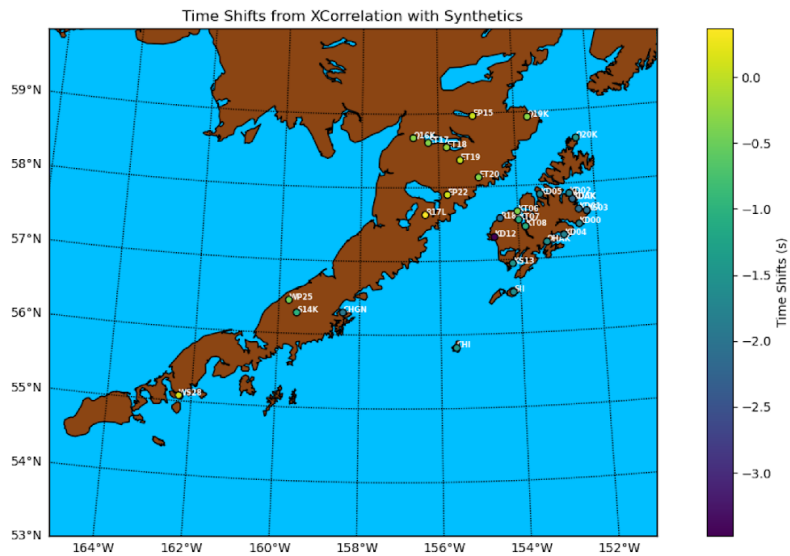


Figure 16: a) time shifts from cross correlation for event 11 plotted according to the colorbar, b) time shifts from cross correlation for event 14. There is a clear pattern in both of early arrivals at the island stations and late arrivals at the land stations.

Discussion:

There are several main points to discuss from the results of this project thus far.

To begin, the original objective of the project was to determine whether or not the triplicated P-phase arrivals due to the Mantle Transition Zone could be discerned from the data collected from the AACSE array, both land and water stations. The early realization that the ocean bottom seismometers require an extra step of response removal (which would require a project of its own), make it unlikely that the data from these particular stations would have discernable phases due to this periodicity, or at least discernable

phases that a researcher would feel comfortable enough trusting without further processing. Again, this is most likely due to the water column periodicity above the stations.

For the remaining stations, the bandpass filter was able to highlight two main observations that led to further analysis: a lack of discernibility for the triplicated phases, and the notable delay times for the land stations. Distinguishing the triplicated phases was the first step of analysis, and due to the land station delay, the seismometers were separated during the fk and vespagram analysis. The fk analysis yielded some very helpful results, in that through the beamforming process it was possible to see several power peaks from the data collected at both the land and island stations.

The vespagram analysis confirmed this result, showing at least two discernable power peaks, and a possible third that is less prominent. This blurring could be due to the fact that a range of azimuthal values was used in constructing the vespagram rather than a single value. As a sanity check, the slownesses from the lower to upper mantle range from around 0.07 s/km to 0.12 s/km respectively, meaning that the calculated values from the vespagrams do make physical sense. The back azimuths align with the calculated value from the known source. Further, the occurrence of the three peaks within the 5 second window around 293 seconds after the event corresponds with the expected triplication from the IASP91 model at the location of the land stations, where the first arrival is at 290.9 seconds and the last is at 293.7. Having done the cross correlation, a difference of 2.1 seconds between the expected and observed first arrival is well within the time shift range calculated.

The values of the slowness calculated for each peak align with the relative slownesses the triplicated phases should have to each other as well. Referring to Figure 1a, between 22 and 23 degrees (where the land stations are epicentrally), the first arrival should have a higher slowness relative to the second and third, and this is the pattern that appears in the vespagram.

For these reasons, it is likely that these three peaks represent the triplicated P phases from the 660 discontinuity of the MTZ.

An interesting pattern arose from the cross correlation with the synthetics. Looking at the time shift maps and comparing them with Figure 2, the stations which experience these time shifts are not only all land stations, but land stations that sit directly in the volcanic regions. It is more than likely that the heterogeneity of the shallow subsurface structure due to these volcanoes has caused this delay in arrival to the stations that sit on the surface, just as is discussed in the Chu et. al paper from which the technique was adopted.

It is important to note that the vespagram analysis was done on the waveforms without applying the time shift from the cross correlation. This is because such a large time shift will most likely get rid of non-regional effects as well as the regional ones, meaning that constructing an accurate velocity structure of the subsurface would be unlikely with these time shifts applied.

This is one of the main reasons OBS' had such a draw for the project in the first place, as they avoid most shallow subsurface structure that would cause these regional effects.

However, as was shown, there are stations that have discernable triplicated phases and help develop a more accurate velocity model of the 660 discontinuity without the additional processing required by the OBS'.

Conclusion:

Over the course of this project, many unexpected challenges arose to what had initially seemed a straightforward modeling problem to me. As I read more of the literature, similarities and differences

between my project and other triplication projects became very apparent. For example, many triplication studies use deeper or larger earthquakes. Larger earthquakes ensure a larger signal is received and recorded at the seismometers, which can help with discerning such minute separate phases. Deeper earthquakes ensure not only penetration through the MTZ, but they reach the surface with a near vertical wavefront meaning that they are less likely to pick up any horizontal heterogeneities in the shallow subsurface, and the vertical component of the seismogram is the only one that needs to be considered. However, it is impossible to control when and how an earthquake happens, and the two events chosen for this project were the only that were initially suitable for the study. Many studies also had a much larger number of stations in the array, so that they were able to look at a small azimuthal range from the event and therefore minimize two dimensional effects that could come from heterogeneities that are only encountered by some of the rays as they travel to their seismometers. Many of the stations used in these studies are also much further inland, which minimizes background noise from ocean waves. In the beginning, I did not realize how significant a portion of the project would have to be devoted to simply finding a suitable event, and from there, filtering the seismograms not only through different frequency bands, but looking at each station individually and determining whether or not there was enough signal to be of use. However, this is a necessary step in the larger question we were trying to answer, and the familiarity I feel I now have with data processing has been integral to my understanding of seismology.

There are several directions in which to go from the results of this project. Research could continue with the filtered waveforms which have discernable triplicated phases from the waveform analysis to construct a velocity model. With the program I developed to construct the vespagrams, I would be interested to run the seismograms recorded at the OBS' through to see if they have salvageable initial P arrivals, for as of now the first 5 seconds after the P arrival is of interest for the triplication. The waveforms do need to have the water column response removed at some point, which is another direction to take this project. The time delays at the land, or rather volcanic stations, could be used to construct a shallow subsurface model of the volcanic region. We could expand the array inland to have a greater number of waveforms to work with, as well as avoid the issues encountered with the OBS'.

Regardless, the conclusions that can be drawn from this project have certain implications for the field of Earth science, in that the discernable triplicated pattern aids in confirming our picture of the Earth's mantle. The waves from the events of interest have probed the Mantle Transition Zone, and made it back to the surface with enough energy to show it. Again, constructing an accurate model of the subsurface is integral to understanding both the physical and chemical structure of the Earth, leading to insights about internal processes which are yet to be fully understood, such as intraplate volcanism. I am quite interested in continuing this research and am excited to further explore the possibilities I feel have been opened by this project.

I would like to thank ELI for giving me the opportunity to participate in undergraduate research, as well as my Research Advisor Geoffrey Abers and the graduate students in my group, Michael Mann and Kiara Daly.

References:

References include triplication literature used for background, AACSE array website, array seismology text for methods, and ObsPy documentation.

All code and data used to generate the figures in this paper is available upon request.

Abers, G. A. "Examining Alaska's earthquakes on land and sea." *Eos* (2019).

Chu, Risheng, Brandon Schmandt, and Don V. Helmberger. "Upper mantle P velocity structure beneath the Midwestern United States derived from triplicated waveforms." *Geochemistry, Geophysics, Geosystems* 13.2 (2012).

<https://doi.org/10.1029/2011GC003818>

Rost, Sebastian, and Christine Thomas. "Array seismology: Methods and applications." *Reviews of geophysics* 40.3 (2002): 2-1.

<https://doi.org/10.1029/2000RG000100>

Wang, Y., Wen, L. & Weidner, D. Array Triplication Data Constraining Seismic Structure and Composition in the Mantle. *Surv Geophys* 30, 355–376 (2009).

<https://doi.org/10.1007/s10712-009-9073-3>

ObsPy Documentation: <https://docs.obspy.org/>